Plumbene on a Magnetic Substrate: A Combined Scanning Tunneling Microscopy and Density Functional Theory Study

Gustav Bihlmayer,[1,*] Jonas Sassmannshausen,[2] André Kubetzka,[2] Stefan Blügel,[1] Kirsten von Bergmann,[2,†] and Roland Wiesendanger[2]

[1]*Peter Grünberg Institut and Institute for Advanced Simulation, Forschungszentrum Jülich and JARA, 52425 Jülich, Germany*

[2]*Department of Physics, University of Hamburg, D-20355 Hamburg, Germany*

(Received 5 September 2019; accepted 11 February 2020; published 24 March 2020)

As a heavy analog of graphene, plumbene is a two-dimensional material with strong spin-orbit coupling effects. Using scanning tunneling microscopy, we observe that Pb forms a flat honeycomb lattice on an Fe monolayer on Ir(111). In contrast, without the Fe layer, a $c(2 \times 4)$ structure of Pb on Ir(111) is found. We use density-functional theory calculations to rationalize these findings and analyze the impact of the hybridization on the plumbene band structure. In the unoccupied states the splitting of the Dirac cone by spin-orbit interaction is clearly observed, while the occupied Pb states are strongly hybridized with the substrate. In a freestanding plumbene we find a band inversion below the Fermi level that leads to the formation of a topologically nontrivial gap. Exchange splitting as mediated by the strong hybridization with the Fe layer drives a quantum spin Hall to quantum anomalous Hall state transition.

DOI: 10.1103/PhysRevLett.124.126401

Since the exotic properties of graphene were discovered about 15 years ago [1], the field of two-dimensional materials in general and honeycomb structures in particular has seen a dramatic increase in popularity [2]. Topological properties in these lattices depend significantly on the strength of spin-orbit coupling (SOC) effects that are notoriously small in graphene, especially at the $\overline{K}$ point [3]. Therefore, although the quantum spin Hall effect was first theoretically predicted for graphene [4], experimentally it was first verified in materials containing heavy elements like HgTe quantum wells [5]. Since then, numerous studies have focused on the synthesis and properties of heavier analogs of graphene like silicene [6], germanene [7], or stanene (Sn) [8]. But the formation of double bonds in this series seems to be restricted to the carbon-based material only and freestanding heavier analogs are considered unlikely to form [9]. Consequently, the first silicene was reported as adlayer on Ag(111) [10] and it is still challenging to balance the interaction with the substrate required for formation with the electronic independence necessary to study the topological properties via electronic transport effects [6]. Furthermore, all heavier analogs of graphene have a tendency to pronounced buckling of their honeycomb structures, resulting in severe changes of the electronic properties as compared to the ideal flat structures [11]. Therefore, it came recently as a welcome surprise that stanene was observed to grow on Cu(111) as a flat honeycomb lattice [12]. Despite the metallic substrate, a topological edge state could be observed on these islands—although 1.3 eV below the Fermi level.

In this quest for heavy honeycomb structures the Pb analog, plumbene, appeared relatively late on the scientific stage. Isoelectronic in its valence shell with C, Si, Ge, and Sn, it is the heaviest graphene analog and expected to show the most pronounced SOC effects [11]. Density functional theory (DFT) studies of plumbene predicted the formation of a buckled honeycomb structure but without band inversion near the Fermi level [13]. Electronically it is similar to a Bi(111) bilayer with less electrons ($Z_{\mathrm{Bi}} = 83$, $Z_{\mathrm{Pb}} = 82$). DFT studies suggested that doping or chemical modification of plumbene [14] might be necessary to achieve topological effects. Maybe it is because of these findings that the quest for plumbene has just begun: A recent study reported on the formation of a Pb honeycomb lattice on Pd(111) grown epitaxially by segregation [15].

Using scanning tunneling microscopy (STM) and DFT we show in this Letter that (i) using an appropriate substrate it is possible to form a flat plumbene lattice and that (ii) the electronic properties of "flat plumbene" are rather exciting: Calculations predict a band inversion in the valence bands that leads to topologically protected edge states. Further, (iii) on the ferromagnetic substrate that enables the formation of plumbene, the induced exchange splitting drives this feature into a quantum anomalous Hall gap. Such exchange coupling opens the way to realize a quantum Hall effect without external magnetic field, a phenomenon envisioned theoretically in the 1980s [16] and only recently realized experimentally [17] at very low temperatures.

We have deposited submonolayer amounts of Pb onto a sample with extended Fe monolayer areas on an Ir(111)

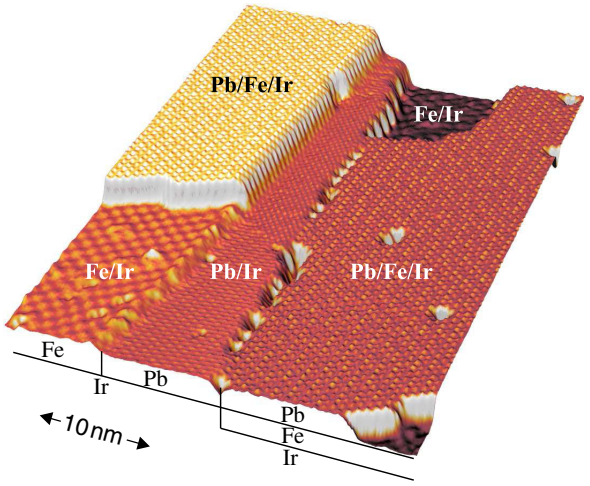

FIG. 1. Pseudo three-dimensional STM image of a sample of Pb on Fe on Ir(111); the different exposed surfaces are labeled. Pb was deposited well below room temperature and grows as monolayer high ordered islands both on the bare Ir surface and on the Fe monolayer on Ir. The superstructure on the pseudomorphic Fe monolayer on Ir is not due to the structure but corresponds to the magnetic signal of the nanoskyrmion lattice. Measurement parameters are $U = +5$ mV, $I = 3$ nA, $T = 4$ K, Cr-bulk tip.

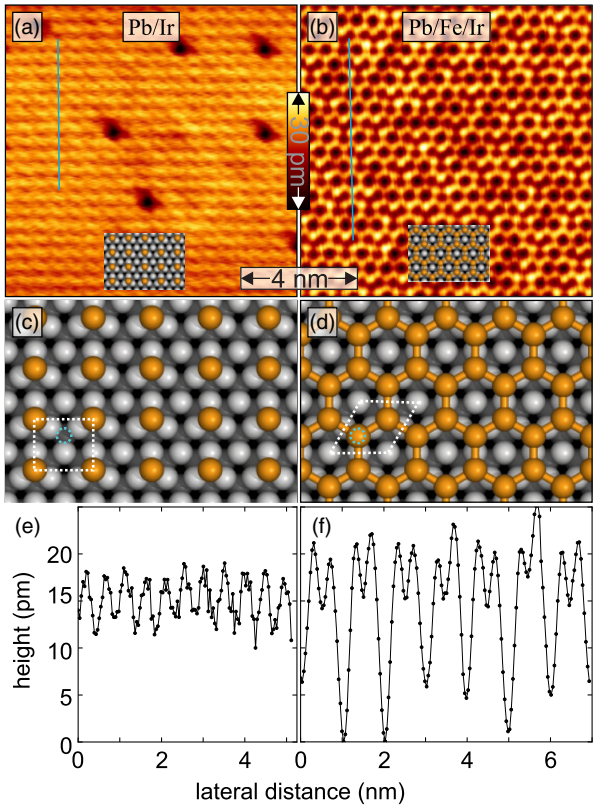

FIG. 2. Closer view constant-current STM images of the Pb monolayer on (a) the bare Ir(111) surface and (b) the Fe monolayer on Ir(111). Both the symmetry and the atomic distances for the two differently ordered Pb monolayers are different and the corresponding structure models are presented in (c) and (d). The white dashed rectangle in (c) refers to the primitive unit cell of the $c(2 \times 4)$ structure and the white dashed diamond in (d) marks the $p(2 \times 2)$ unit cell; blue dashed circles mark positions that are empty for a lower atom-density configuration and occupied for a higher atom-density configuration (see text). Panels (e) and (f) show the height profiles along the lines indicated in (a) and (b), respectively. Measurement parameters are (a) $U = +10$ mV, $I = 1.5$ nA, (b) $U = +5$ mV, $I = 2$ nA, both (a) and (b) $T = 4$ K, Cr-bulk tip. Information on the bias dependence is provided in the Supplemental Material [21], Fig. S1.

single crystal surface; see overview STM image in Fig. 1. Because we observed severe intermixing of Pb and Fe for Pb growth at room temperature, we have cooled the Fe/Ir(111) to about 140 K prior to the Pb deposition [18], which results in large and well-ordered patches of Pb both on the bare Ir(111) and the Fe-covered Ir(111); see labels for the different layers in Fig. 1. The Fe monolayer grows pseudomorphically in fcc stacking on the Ir(111) substrate, and in this spin-polarized STM measurement [19] the observed roughly square superstructure with a periodicity of about 1 nm originates from the magnetic nanoskyrmion lattice [20]. No magnetic signal has been observed on the Pb monolayers.

A closer view of the Pb deposited directly on the Ir and on Fe/Ir is shown in Figs. 2(a) and 2(b), respectively. Here the superstructures are of structural origin. Because of the large lattice mismatch of Pb and Ir, the Pb overlayers are not pseudomorphic, but instead form layers with reduced atom density. Nevertheless, the Pb superstructures are commensurate with the substrate and atoms reside at specific adsorption sites of the Ir or Fe/Ir, an indication that the Pb-substrate interaction is comparable to the Pb-Pb interaction.

On Ir(111) we find a $c(4 \times 2)$ Pb overlayer that can be described with a rectangular unit cell, see white dashed rectangle in Fig. 2(c), like in the graphene intercalated Pb films on Ir [31]. The Pb atoms all occupy the same adsorption sites and the Pb-Pb distances are 4.70 and 5.43 Å for the two orthogonal directions. For symmetry reasons, three rotational domains are found on a larger scale.

In contrast, on the Pb/Fe/Ir we find a honeycomb arrangement of the Pb atoms, see experimental data and corresponding structure model in Figs. 2(b) and 2(d); i.e., the Pb grows on Fe/Ir(111) in the modification of plumbene. The structural $p(2 \times 2)$ unit cell (see white dashed diamond) contains two Pb atoms that adsorb in a fcc and a hcp site. The Pb atom density of this honeycomb plumbene layer is twice that of the $c(4 \times 2)$ Pb overlayer on Ir. Since both the Fe/Ir and the Ir(111) surface have the same symmetry and identical atomic distances, the difference in the Pb overlayer structures cannot originate from geometrical reasons. While the structural unit cell of the honeycomb has lattice vectors with a length of 5.43 Å, the Pb-Pb distance is only $\sqrt{6}/3 a_{\mathrm{Ir}} = 3.13$ Å, i.e., more than 10% shorter than in fcc Pb ($a_{\mathrm{Pb}}/\sqrt{2} = 3.52$ Å). Comparing

graphene with diamond a similar contraction of bond distances (1.42 Å versus 1.55 Å) can be observed, suggesting that the Pb—Pb bond is modified in a similar way as the C—C bond for the two different allotropes. We note that the plumbene reported in Ref. [15] has a much smaller lattice constant of 4.8 Å, close to the theoretically obtained value of 4.93 Å [13]. But while the calculations at this lattice constant predict a buckled structure, our line profiles in Fig. 2(f) show that we obtained a flat honeycomb layer. Figure 2 also reveals the presence of a significant amount of defects that is not present in Pb on Ir(111). In the Supplemental Material [21] more data are shown that suggest that these defects are Pb vacancies.

Using density-functional theory we study the energetics of different Pb monolayers on Ir(111) and Fe/Ir(111). Based on the experimental findings, we compare four possible arrangements of Pb at these surfaces: $p(2\times2)$ and $c(2\times4)$ unit cells (u.c.) with one or two Pb atoms per cell; i.e., the structures shown in Figs. 2(c) and 2(d) with and without the atoms at positions marked by the dashed blue circle.

Comparing fcc and hcp adsorption sites, a single Pb atom on Ir(111) forming a $p(2\times2)$ or $c(2\times4)$ structure always prefers the fcc site by 49 meV/Pb. The $p(2\times2)$ and $c(2\times4)$ arrangements differ by only 5 meV in favor of the former. The fact that experimentally a $c(2\times4)$ structure is observed might be related to neglected effects from the vibrational entropy or limitations of the computational method. To put two Pb atoms into a $c(2\times4)$ u.c., however, requires 54 meV/Pb more energy than a single one, and the formation of a Pb honeycomb lattice in the $p(2\times2)$ cell is energetically 216 meV/Pb more expensive than the $c(2\times4)$ arrangement with the same atom density. Thus, on Ir(111) a low Pb atom density with larger Pb-Pb distances is energetically favorable as found in the experiments reported here and in the graphene-covered system [31]. Our STM simulations based on the local density of states also show good agreement with the experimental images (see Supplemental Material [21], Fig. S2).

This high energy cost to form a Pb honeycomb structure on Ir(111) is contrasted by the energetics of Pb on Fe/Ir(111): here the honeycomb lattice is favored by 11 meV/Pb atom over the $c(2\times4)$ structure with the same areal Pb density (2 Pb/u.c.) and by 44 meV over a $p(2\times2)$ arrangement with only one Pb atom per unit cell. The structural relaxation shows that the honeycomb layer is almost completely flat with a corrugation of 0.002 Å. In all cases we assumed a ferromagnetic order of the Fe layer. Test calculations of Fe layers with antiferromagnetic nearest neighbor interactions lead to much higher total energies (see Supplemental Material [21]). A similar magnetic hardening was observed when coronene is adsorbed on the Fe/Ir(111) nanoskyrmion lattice [32] and can occur generally when p electrons of molecules interact with a magnetic layer underneath [33].

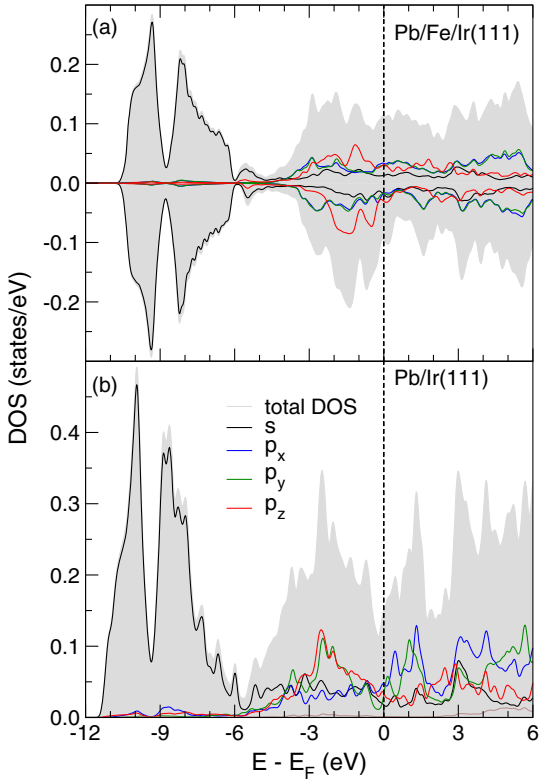

FIG. 3. (a) Orbitally resolved DOS of the Pb atoms in the honeycomb structure on Fe/Ir(111). The total Pb DOS is shown as gray background, and the s, p_x, p_y, and p_z contributions are shown in black, blue, green, and red, respectively. Positive and negative values correspond to majority and minority spins, respectively. (b) The same quantities for the Pb honeycomb lattice on Ir(111).

To understand the radically different energetics of Pb on Ir(111) and on Fe/Ir(111), we analyze the orbitally resolved density of states (DOS) for the honeycomb structure in Fig. 3. In the case of the Fe/Ir(111) substrate, we see that the DOS of the Pb p_x and p_y states is almost degenerate and rather featureless near the Fermi level, while the p_z states show characteristic peaks at or below 1 eV binding energy where the minority Fe states are located (the majority states of Fe are peaked between 2 and 3 eV binding energy, see Supplemental Material [21], Fig. S3). While in this case the in-plane and out-of-plane oriented p orbitals of Pb seem rather decoupled (as expected from a 2D structure bonded by p_z orbitals to the substrate), in the Pb/Ir(111) case we find a completely different orbital arrangement with p_y and p_z orbitals bonding to the Ir substrate. Although also in this case an almost flat Pb honeycomb structure is obtained, the involved orbitals are completely different. Therefore, it can be concluded that the hybridization with the Fe states, that are available in the energy range of the Pb p_z states, is responsible for the formation of the 2D Pb honeycomb lattice.

Turning now to the band structure of Pb on Fe/Ir(111), it is instructive to investigate first the plumbene layer without the substrate (black lines in Fig. 4). Below the Fermi level

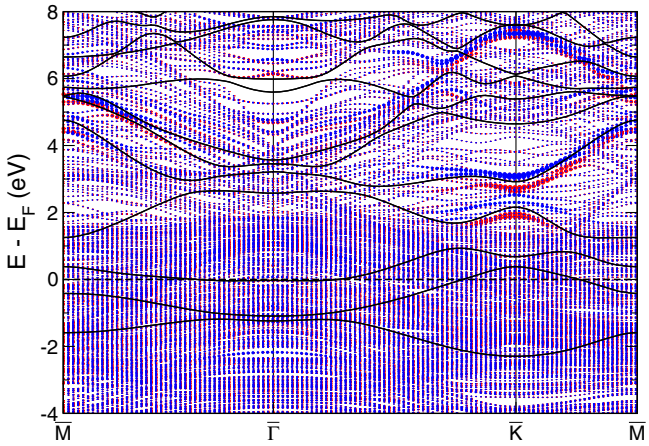

FIG. 4. Red and blue: Sign of the spin polarization of the Pb states of a Pb honeycomb structure on Fe/Ir(111). Spin-orbit coupling is included and the spin-quantization axis is assumed to be normal to the surface. In black the band structure of a freestanding plumbene layer with the same structure as the supported one is shown.

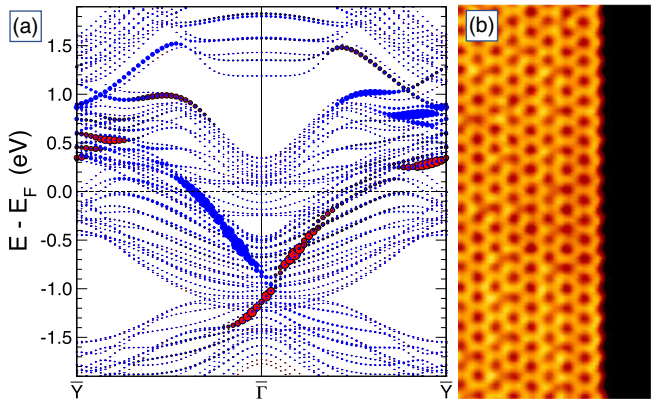

FIG. 5. (a) Band structure of a freestanding, edge-hydrogenated plumbene ribbon in an external magnetic field. The size of the dots marks the weight of the states on one of the zigzag edges, the color indicates the spin character. (b) Constant-current STM image of the typical zigzag configuration of the edge of a plumbene island on Fe/Ir; measurement parameters are $U = -10$ mV, $I = 2$ nA, $T = 4$ K, Cr-bulk tip.

two rather flat bands can be found and the p_z states form a hole pocket around the $\overline{K}$ point, compensated by a shallow electron pocket of the antibonding $p_{x,y}$ states at $\bar{\Gamma}$. At around 1 eV binding energy the bonding $p_{x,y}$ states show a band inversion with the p_z states at the $\bar{\Gamma}$ point, very similar to the band inversion observed for stanene in Ref. [12]. On the metallic substrate these Pb states are, however, strongly hybridized with the Fe d states and—as evident from Fig. 4—only above the Fermi level the individual Pb states can be identified again. The induced spin splitting in these states is substantial, between 0.2 and 0.4 eV. This can be seen best at the $\overline{K}$ point, where the Dirac-type band crossing is lifted by SOC (for the band structure without SOC, see Supplemental Material [21], Fig. S4).

Although the features of the Pb bands are blurred by hybridization, it is of interest to study the consequences of the abovementioned band inversion of plumbene at the $\bar{\Gamma}$ point. Strong SOC in Pb opens a 150 meV band gap between the states that hosts topologically protected edge states. In the calculation of the unsupported, edge-hydrogenated plumbene zigzag ribbon the linear dispersion of the edge state is clearly visible in the gap (see Supplemental Material [21], Fig. S5). This is a clear signature of the quantum spin Hall effect (although in the occupied states) as expected from the parity analysis of the bands. Since the Fe substrate induces a strong exchange field in the plumbene, we can further look for the appearance of a quantum anomalous Hall gap in the system. To simulate the effect of the exchange field in the unsupported plumbene ribbon, we add an external magnetic field in the calculation that reproduces the spin splitting of the Pb bands seen in Fig. 4. Although in the projection on the edge the spin-split band edges now overlap, the single, spin-polarized edge channel is clearly visible in this system (Fig. 5). At the Fermi level the signature of this state is masked by the large DOS created by other states; therefore the edge does not appear brighter than the film in the STM image in Fig. 5(b). At more negative bias voltages (Fig. S1b of Ref. [21]) a rim is visible, but this could also be related to conventional edge states.

We have shown experimental and theoretical evidence that the heaviest member of the graphene family, plumbene, can be prepared on an Fe layer on Ir(111). Selective hybridization of the Pb p_z states with the Fe minority d states stabilizes the honeycomb structure, while on bare Ir(111) a rectangular $c(2 \times 4)$ Pb layer is formed. The ferromagnetic substrate induces a significant exchange splitting in the plumbene. Freestanding plumbene with this lattice constant shows a band inversion in the occupied states and topologically protected edge states. With the exchange splitting this quantum spin Hall gap is changed into a quantum anomalous Hall gap providing a protected charge channel. Although on the metallic substrate these states will be considerably broadened and not accessible to transport measurements, with a modified substrate this system might be a nice platform to study the properties of edge states of a Chern insulator.

We would like to thank Niklas Romming for technical assistance with the experiments. We gratefully acknowledge the Priority Program SPP 1666 of the Deutsche Forschungsgemeinschaft (DFG, German Research Foundation) and the computing time on the JURECA supercomputer of the Jülich Supercomputing Centre (JSC). Financial support from the ERC Advanced Grant ADMIRE is gratefully acknowledged. K. v. B. and A. K. acknowledge financial support from the DFG Grants No. 418425860, No. 402843438, and No. 408119516.

*g.bihlmayer@fz-juelich.de
†kbergman@physnet.uni-hamburg.de

[1] K. S. Novoselov, A. K. Geim, S. V. Morozov, D. Jiang, Y. Zhang, S. V. Dubonos, I. V. Grigorieva, and A. A. Firsov, Science **306**, 666 (2004).
[2] A. H. Castro Neto, F. Guinea, N. M. R. Peres, K. S. Novoselov, and A. K. Geim, Rev. Mod. Phys. **81**, 109 (2009).
[3] C.-C. Liu, W. Feng, and Y. Yao, Phys. Rev. Lett. **107**, 076802 (2011).
[4] C. L. Kane and E. J. Mele, Phys. Rev. Lett. **95**, 226801 (2005).
[5] M. König, S. Wiedmann, C. Brüne, A. Roth, H. Buhmann, L. W. Molenkamp, X.-L. Qi, and S.-C. Zhang, Science **318**, 766 (2007).
[6] A. Molle, C. Grazianetti, L. Tao, D. Taneja, M. H. Alam, and D. Akinwande, Chem. Soc. Rev. **47**, 6370 (2018).
[7] L. Zhang, P. Bampoulis, A. N. Rudenko, Q. Yao, A. van Houselt, B. Poelsema, M. I. Katsnelson, and H. J. W. Zandvliet, Phys. Rev. Lett. **116**, 256804 (2016).
[8] F.-F. Zhu, W.-J. Chen, Y. Xu, C.-L. Gao, D.-D. Guan, C.-H. Liu, D. Qian, S.-C. Zhang, and J.-F. Jia, Nat. Mater. **14**, 1020 (2015).
[9] R. Hoffmann, Angew. Chem. Int. Ed. **52**, 93 (2013).
[10] P. Vogt, P. De Padova, C. Quaresima, J. Avila, E. Frantzeskakis, M. C. Asensio, A. Resta, B. Ealet, and G. Le Lay, Phys. Rev. Lett. **108**, 155501 (2012).
[11] Z.-Q. Huang, C.-H. Hsu, F.-C. Chuang, Y.-T. Liu, H. Lin, W.-S. Su, V. Ozolins, and A. Bansil, New J. Phys. **16**, 105018 (2014).
[12] J. Deng, B. Xia, X. Ma, H. Chen, H. Shan, X. Zhai, B. Li, A. Zhao, Y. Xu, W. Duan, S.-C. Zhang, B. Wang, and J. G. Hou, Nat. Mater. **17**, 1081 (2018).
[13] X.-L. Yu, L. Huang, and J. Wu, Phys. Rev. B **95**, 125113 (2017).
[14] H. Zhao, C.-W. Zhang, W.-X. Ji, R.-W. Zhang, S.-S. Li, S.-S. Yan, B.-M. Zhang, P. Li, and P.-J. Wang, Sci. Rep. **6**, 20152 (2016).
[15] J. Yuhara, B. He, N. Matsunami, M. Nakatake, and G. Le Lay, Adv. Mater. **31**, 1901017 (2019).
[16] F. D. M. Haldane, Phys. Rev. Lett. **61**, 2015 (1988).
[17] C.-Z. Chang *et al.*, Science **340**, 167 (2013).
[18] J. Sassmannshausen, A. Kubetzka, P.-J. Hsu, K. von Bergmann, and R. Wiesendanger, Phys. Rev. B **98**, 144443 (2018).
[19] R. Wiesendanger, Rev. Mod. Phys. **81**, 1495 (2009).
[20] S. Heinze, K. von Bergmann, M. Menzel, J. Brede, A. Kubetzka, R. Wiesendanger, G. Bihlmayer, and S. Blügel, Nat. Phys. **7**, 713 (2011).
[21] See Supplemental Material at http://link.aps.org/supplemental/10.1103/PhysRevLett.124.126401 for computational details, information on the magnetic structure and impact of defects, and additional figures, which includes Refs. [22–30].
[22] E. Wimmer, H. Krakauer, M. Weinert, and A. J. Freeman, Phys. Rev. B **24**, 864 (1981).
[23] M. De Santis, Y. Gauthier, H. C. N. Tolentino, G. Bihlmayer, S. Blügel, and V. Langlais, Phys. Rev. B **75**, 205432 (2007).
[24] S. H. Vosko, L. Wilk, and M. Nusair, Can. J. Phys. **58**, 1200 (1980).
[25] C. Li, A. J. Freeman, H. J. F. Jansen, and C. L. Fu, Phys. Rev. B **42**, 5433 (1990).
[26] N. Romming, C. Hanneken, M. Menzel, J. E. Bickel, B. Wolter, K. von Bergmann, A. Kubetzka, and R. Wiesendanger, Science **341**, 636 (2013).
[27] D. Iaia, A. Kubetzka, K. von Bergmann, and R. Wiesendanger, Phys. Rev. B **93**, 134409 (2016).
[28] V. Caciuc, N. Atodiresei, and S. Blügel, Phys. Rev. Mater. **2**, 084001 (2018).
[29] K. von Bergmann, S. Heinze, M. Bode, G. Bihlmayer, S. Blügel, and R. Wiesendanger, New J. Phys. **9**, 396 (2007).
[30] Q. Wu, S. Zhang, H.-F. Song, M. Troyer, and A. A. Soluyanov, Comput. Phys. Commun. **224**, 405 (2018).
[31] F. Calleja, H. Ochoa, M. Garnica, S. Barja, J. J. Navarro, A. Black, M. M. Otrokov, E. V. Chulkov, A. Arnau, A. L. V. de Parga, F. Guinea, and R. Miranda, Nat. Phys. **11**, 43 (2015).
[32] J. Brede, N. Atodiresei, V. Caciuc, M. Bazarnik, A. Al-Zubi, S. Blügel, and R. Wiesendanger, Nat. Nanotechnol. **9**, 1018 (2014).
[33] R. Friedrich, V. Caciuc, N. S. Kiselev, N. Atodiresei, and S. Blügel, Phys. Rev. B **91**, 115432 (2015).